

Biocatalysis

Covalent Organic Framework Nanosheets for the Assembly of Efficient Membrane Bioreactors

Jingxu Han⁺, Zhiwei Xing⁺, Qing Guo, Di Wu, Zhuozhi Lai, Xiaoxiao Cheng, Zhifeng Dai,^{*} Yubing Xiong, Xiangju Meng, Shengqian Ma, Feng-Shou Xiao, and Qi Sun^{*}

Abstract: Immobilizing fragile enzymes in porous materials holds significant potential for biocatalysis but encounters challenges such as mismatched enzyme size and pore structure of host materials, along with harsh assembly conditions that can denature enzymes. Herein, we present a versatile strategy for constructing membrane bioreactors through water-mediated, vacuum-assisted layer-by-layer assembly of covalent organic framework (COF) nanosheets with enzymes. This method effectively addresses pore size limitations, preserves enzyme activity, and promotes convective transport of reactants to active sites, while shielding enzymes from harmful by-products through rapid transport in continuous membrane catalysis. The optimized bioreactor achieves a 1018-fold increase in relative activity compared to free enzymes in batch reactions, completing substrate conversion in just 7.95 s, and demonstrating enhanced stability.

tuating temperatures or harsh chemical environments.^[6–11] To address these challenges, enzyme immobilization techniques have emerged as a powerful tool to enhance enzyme stability, activity, and reusability.^[12–21] Despite significant advancements, batch enzymatic reactions still face challenges. Enzymes in such systems are often exposed to harmful by-products for prolonged periods, increasing the risk of deactivation. To mitigate this, continuous enzymatic processes using membrane bioreactors have been developed.^[22–28] These systems typically retain enzymes via low molecular weight cut-off membranes or covalent modifications. Although effective, such approaches come with notable trade-offs, including high energy consumption for filtration and potential enzyme damage during the modification process. A promising alternative is *in situ* biomimetic mineralization, where enzymes are encapsulated within protective metal-organic framework (MOF) membranes.^[29] However, current applications have been largely limited to zeolite imidazolate framework-8 (ZIF-8), which has a narrow pore size of 3.8 Å, restricting access to larger reagents and limiting practical applications. Thus, a versatile and effective strategy for the construction of bioactive membrane reactor is highly desired.

Covalent organic framework (COF) nanosheets emerge as ideal candidates for such applications due to their well-defined structures, functional versatility, and intrinsic porosity.^[30–36] Their excellent water dispersibility and ability to form membranes further enhance their applicability in chemical separation, catalysis, energy conversion, and sensing.^[37–44] By assembling COF nanosheets with enzymes using a water-mediated, vacuum-assisted layer-by-layer approach, it is no longer necessary to precisely match the pore size of the COF with the enzyme dimensions. This integration improves mass transfer and enzyme accessibility by leveraging both the intrinsic porosity of the COF nanosheets and the interlayer spaces created during the assembly process. Furthermore, the tunable chemical compositions of COFs allow for the customization of the enzyme microenvironment to achieve optimal catalytic performance (Figure 1).

To assess the potential of COF nanosheets in constructing membrane bioreactors, we conducted a proof-of-concept study involving the encapsulation of lipase, selected for its versatile catalytic properties.^[45–47] The optimized membrane bioreactor demonstrated exceptional catalytic efficiency, achieving complete conversion in just 7.95 s at room temperature in the kinetic resolution of racemic secondary alcohols with vinyl acetate. This performance surpassed both free enzymes and COF powder biocomposites, delivering

Introduction

Enzymes are highly efficient and selective catalysts, essential for promoting sustainable manufacturing processes.^[1–5] Despite their advantages, enzymes are inherently fragile, with activity and selectivity often compromised under fluctuating


[*] J. Han⁺, Prof. Z. Dai, Prof. Y. Xiong
Key Laboratory of Surface & Interface Science of Polymer Materials of Zhejiang Province, School of Chemistry and Chemical Engineering, Zhejiang Sci-Tech University, Hangzhou 310018, China
E-mail: daizhifeng1988@163.com

Z. Xing⁺, Q. Guo, D. Wu, Z. Lai, Prof. F.-S. Xiao, Prof. Q. Sun
Zhejiang Provincial Key Laboratory of Advanced Chemical Engineering Manufacture Technology, College of Chemical and Biological Engineering, Zhejiang University, Hangzhou 310027, China
E-mail: sunqichs@zju.edu.cn

X. Cheng, X. Meng
Department of Chemistry, Zhejiang University, Hangzhou 310027, China

Prof. S. Ma
Department of Chemistry, University of North Texas, 1508 W Mulberry St, Denton TX 76201, USA

[⁺] Both authors contributed equally to this work.

 Additional supporting information can be found online in the Supporting Information section

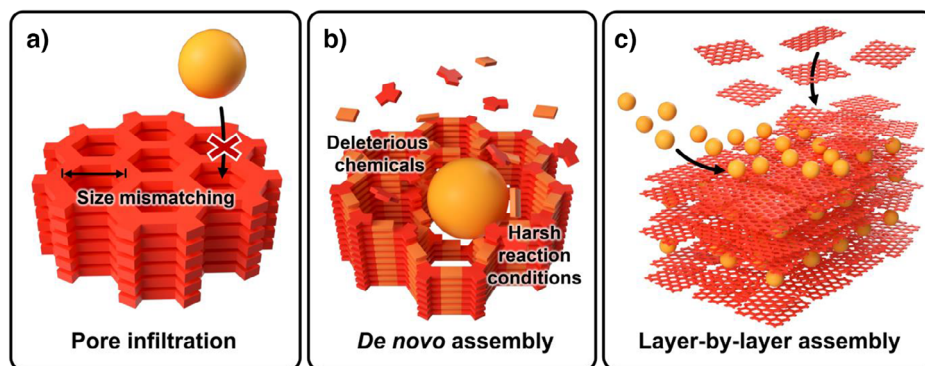


Figure 1. Overview of various enzyme immobilization techniques. a) Direct pore infiltration, which requires the pore size of the host material to be larger than the dimensions of the enzyme for effective immobilization. b) *De novo* assembly, typically involving harsh chemical reactions and conditions that may negatively impact enzyme activity. c) Layer-by-layer assembly using COF nanosheets with enzymes, along with the associated advantages.

turnover frequencies (TOFs) that were 1018-fold and 254-fold higher, respectively. Beyond its remarkable catalytic efficiency, the membrane bioreactor enabled rapid removal of reaction products, further enhancing enzyme stability and activity across multiple reactions. Notably, this versatile immobilization approach is not limited to specific enzymes or COF types, providing a universal platform for engineering advanced membrane bioreactors.

Results and Discussion

Given the demonstrated enhanced efficiency of lipase with hydrophobic substrates, we selected COF nanosheets synthesized from 1,3,5-tris(4-aminophenyl)benzene (Tab) and 2,5-dimethoxyterephthalaldehyde (Dma). This choice was motivated by the hydrophobicity, chemical stability, and mesoporous structure of the resulting COF material, which are advantageous for mass transport.^[48] The COF-TabDma nanosheets were prepared using a single-phase solution method facilitated by scandium trifluoromethanesulfonate ($\text{Sc}(\text{OTf})_3$) (Figure 2a). The formation of nanosheets was indicated by the Tyndall light-scattering effect observed in the suspension (Figure 2a, inset, and Figure S1). Comprehensive characterization techniques further validated the morphology and structural properties of the COF-TabDma nanosheets. Scanning electron microscopy (SEM) revealed a uniform lamellar structure (Figure 2b), while atomic force microscopy (AFM) measured their thickness to be approximately 4.5 nm (Figure 2c). Additionally, transmission electron microscopy (TEM) showed a smooth, nearly transparent, flake-like morphology, consistent with their atomically thin structure (Figure 2d).

The membrane bioreactors were fabricated using a vacuum-assisted layer-by-layer stacking method on polyacrylonitrile (PAN) ultrafiltration membranes. The process involved sequential filtrations of a diluted COF nanosheet aqueous solution, followed by enzyme solutions containing Amano lipase PS from *Burkholderia cepacia* at varying concentrations (0, 2500, 5000, and 10 000 ppm). This cycle was repeated to build layer-by-layer assembly structures

between COF nanosheets and enzyme molecules, with an additional COF nanosheet layer applied to shield the enzyme from environmental exposure (Figure 2e). The choice of PAN membranes was motivated by their uniform nanoscale pores, which facilitate effective nanosheet deposition and layering. Experimental results demonstrated that membranes fabricated within a pressure range of 0.3–0.9 bar exhibited consistent performance metrics. The resulting membranes, designated as $\text{E}_x@\text{COF-}y/\text{PAN}$ (where x represents enzyme concentration and y the number of layering cycles), exhibited uniform coloration ranging from orange-red to brown (Figure S2). Characterization through scanning electron microscopy (SEM) revealed a continuous, pinhole-free structure, with membrane thickness increasing proportionally from 14 to 51 μm as the number of layering cycles and enzyme concentration increased (Figures 2f and S3–S7). Further structural insights were obtained from high-resolution TEM, which displayed distinct periodic crystal lattice fringes with 2.65 nm 1D pore channels corresponding to the (010) facet of the COF material, crystal lattice fringes with 2.65 nm 1D pore channels corresponding to the (010) facet of the COF material, indicating high crystallinity and porosity (Figures 2g, S8). This observation was further validated by powder X-ray diffraction (PXRD), which confirmed that the COF membrane retained its crystallinity even after enzyme incorporation (Figure S9).

Fourier transform infrared (FT-IR) spectroscopy of $\text{E}_0@\text{COF-15}$ and its precursors exhibited notable spectral shifts. The appearance of an imine $\text{C}=\text{N}$ stretch at 1610 cm^{-1} along with the vanishing of aldehydic $\text{C}=\text{O}$ stretch vibrations from Dma and $\text{N}-\text{H}$ stretch vibrations from Tab, suggesting a high degree of polymerization (Figure S10).^[49] Moreover, the emergence of an amide I band at 1660 cm^{-1} , associated with $\text{C}=\text{O}$ stretch vibrations, confirmed the successful immobilization of lipase. The intensity of this band increased with the enzyme solution concentration, reflecting higher enzyme encapsulation (Figure S11). Additionally, the shift of the amide I band to a higher wavenumber in the immobilized state, compared to the free enzyme, suggested a conformational change in lipase, likely to an enzymatically active open-lid conformation within

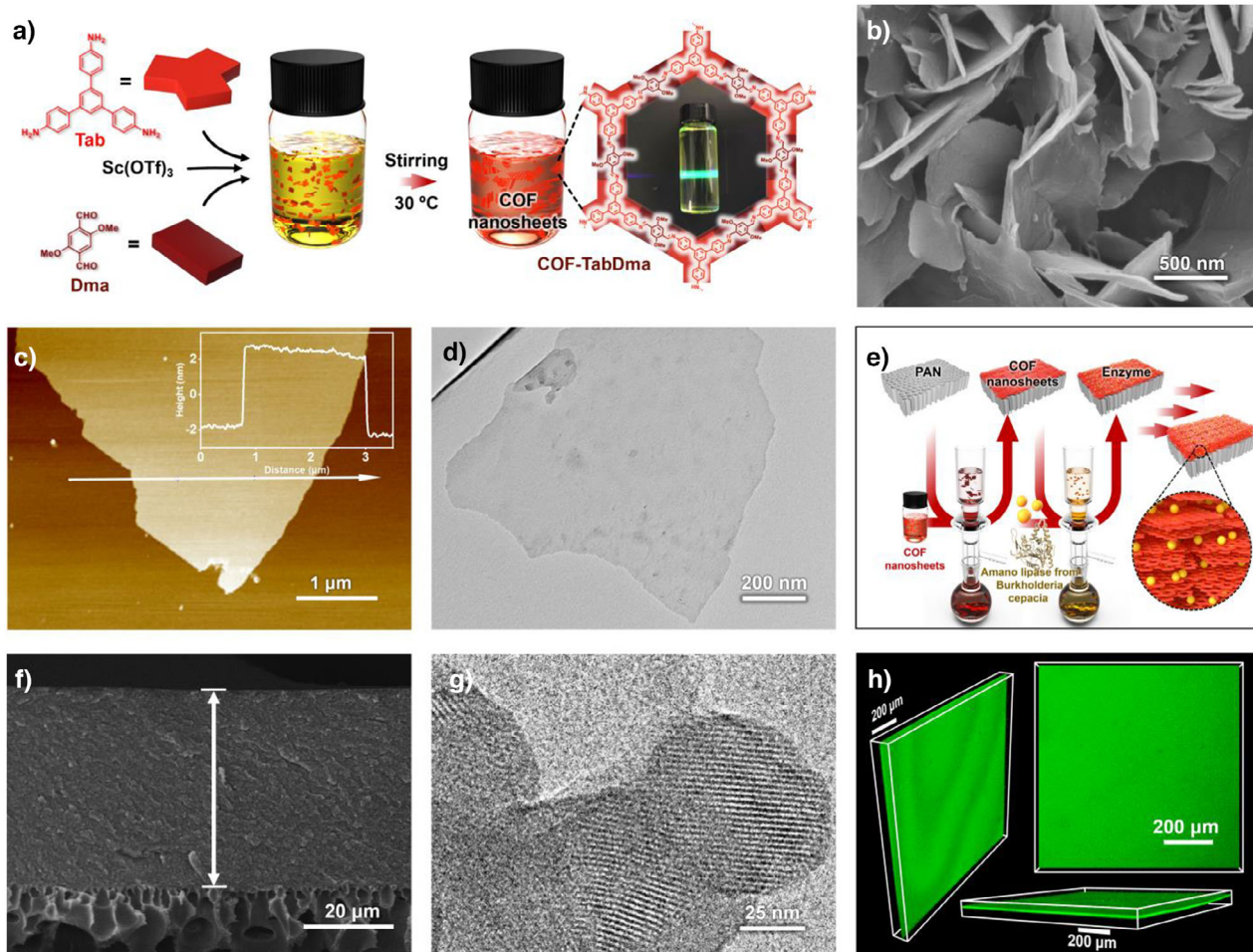


Figure 2. Materials synthesis and characterization. a) Schematic illustration of the synthesis of COF-TabDma nanosheets; inset shows Tyndall light-scattering effect in the suspensions. b) SEM image showcasing the structure of COF-TabDma nanosheets. c) AFM image of COF-TabDma nanosheets with an inset showing the height profile; the arrow indicates the scanning direction. d) TEM image of the COF-TabDma nanosheets. e) Schematic depiction of the layer-by-layer assembly strategy used in constructing the membrane bioreactor. f) Cross-sectional SEM image of the $E_{5000}@COF-15/PAN$ membrane, showing a thickness of 45 μm . g) High-resolution TEM image of the COF membrane assembled by the COF nanosheets. h) CLSM images of the fluorescein isothiocyanate-labeled $E_{5000}@COF-15/PAN$ membrane.

the hydrophobic membrane environment. This change is attributed to hydrophobic interactions.^[50–53]

To assess the distribution of lipase within the composite membrane, we employed fluorescein isothiocyanate (FITC) to label the enzyme molecules for visualization. Confocal laser scanning microscopy (CLSM) revealed a uniform distribution of FITC-labeled lipase, visible as green fluorescence across the $E_x@COF-y/PAN$ membrane (Figure 2h). This indicated a homogeneous enzyme dispersion within the COF layers. A comparative experiment highlighted the advantages of the layer-by-layer assembly method. When COF nanosheets were first formed into a membrane via vacuum filtration, followed by enzyme filtration, CLSM images showed limited enzyme localization, with enzyme molecules confined primarily to the membrane surface. This comparison demonstrated that the layer-by-layer approach significantly improves immobilization efficiency, enhancing enzyme protection and activity (Figure S12).

Thermogravimetric analysis (TGA) of the membrane bioreactors showed weight loss between 270 and 335 $^{\circ}C$, with

the extent of loss increasing proportionally with enzyme precursor concentration. This trend indicated that higher enzyme concentrations resulted in greater enzyme embedding within the membrane (Figure S13). To quantify enzyme loading, the COF membranes were digested, and nuclear magnetic resonance (NMR) analysis was performed (Figure S14). Results demonstrated that enzyme loading could be precisely controlled by adjusting enzyme solution concentration: higher precursor concentrations resulted in higher loadings. For instance, $E_{2500}@COF-15/PAN$, $E_{5000}@COF-15/PAN$, and $E_{10000}@COF-15/PAN$ exhibited enzyme loadings of 16.4 wt.%, 21.9 wt.%, and 29.1 wt.%, respectively. Notably, a linear relationship was observed between membrane thickness and enzyme loading, suggesting that enzyme molecules predominantly occupy the interlayer spaces of the COF sheets rather than the pores (Figure S15). To verify the uniformity of enzyme dispersion, membranes assembled with different layer-by-layer cycles were compared. $E_{5000}@COF-4/PAN$, $E_{5000}@COF-8/PAN$, and $E_{5000}@COF-15/PAN$ showed enzyme loadings of 20.7 wt.%, 20.2 wt.%, and 21.9 wt.%, respectively,

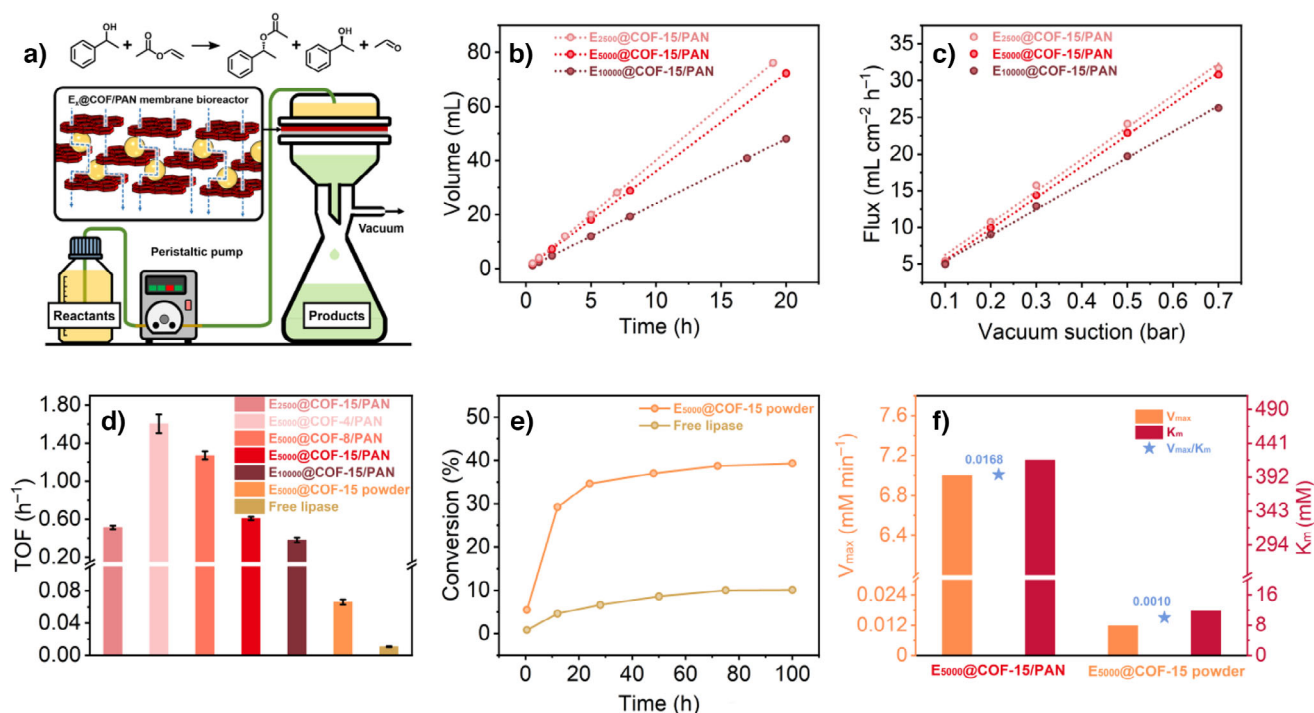


Figure 3. Comparative enzymatic performance of membrane bioreactors and batch systems. a) Schematic illustration of the experimental setup for membrane catalysis. b) Time-dependent permeate volumes under vacuum suction of 0.05 bar for various membrane bioreactors. c) Membrane flux as a function of vacuum suction pressure. d) Comparative catalytic efficiency across different systems after 30 min of reaction. Error bars represent the standard deviation from three independent trials for each catalytic system. e) Time-dependent conversion of 1-phenylethanol catalyzed by $E_{5000}@COF-15$ powder and the free lipase. Reactions were performed with a 1.8 mL solution of 1-phenylethanol (5 mM) and vinyl acetate (15 mM) in hexane, stirred at room temperature. The reaction volume correlates with the permeate volume of the $E_{5000}@COF-15/PAN$ membrane reactor, using 8.0 mg of $E_{5000}@COF-15$ powder (equivalent to the biocomposite enzyme in the membrane) and 1.8 mg of free enzyme (matching enzyme loading). Product yields were determined using gas chromatography (GC), with values validated through three independent experiments. f) Kinetic parameter comparison between $E_{5000}@COF-15/PAN$ and $E_{5000}@COF-15$ powder.

confirming consistent and homogeneous enzyme distribution across the layers. Furthermore, the enzyme exhibited excellent integration and stability with the COF nanosheets. Even after extensive washing with water, $E_{5000}@COF-15/PAN$ retained 19.9 wt.% enzyme content, demonstrating the robustness of the immobilization method.

To assess the enzymatic performance of $E_x@COF-y/PAN$, we conducted the kinetic resolution of racemic secondary alcohols, driven by the need for enantiomerically pure alcohols in the industrial and pharmaceutical applications, which can be achieved with high enantioselectivity through lipase-mediated catalysis. 1-Phenylethanol was chosen as the model substrate due to the high demand for its (*S*)-enantiomer in these fields.^[54–56] The experiments were performed using a custom-built dead-end microfiltration device with an effective area of 1.77 cm^2 . The feed chamber was supplied with a hexane solution containing 5 mM 1-phenylethanol and 15 mM vinyl acetate using a peristaltic pump (Figure 3a). Vacuum suction was applied to facilitate the reaction. The bioreactor demonstrated stable operational performance, as evidenced by a linear relationship between flow volume and time under constant pressure, along with a proportional increase in membrane flux with increasing pressure (Figure 3b,c).

The $E_{5000}@COF-15/PAN$ membrane reactor demonstrated exceptional performance, achieving a theoretical conversion

of 50.0% for 1-phenylethanol, with an enantiomeric excess (ee) exceeding 99.0% (Figure S16). At a vacuum suction of 0.05 bar, the membrane reactor displayed a flux of 407.6 $\text{L m}^{-2} \text{h}^{-1} \text{bar}^{-1}$. Using Equation (1), the estimated contact time required for complete conversion was only 7.95 s:^[57,58]

$$t_R = \frac{V_{Reactor}}{k} = \frac{\pi r^2 h}{k} \quad (1)$$

where, t_R denotes the maximum reaction time, $V_{Reactor}$ is the total volume of the membrane, k represents the slope of the reactant flow volume over time, r is the radius of the membrane reactor, and h is the thickness of the membrane. In contrast, $E_{2500}@COF-15/PAN$ and $E_{10000}@COF-15/PAN$ membranes displayed lower conversion rates of 36.0% and 44.9%, respectively, with flux values of 475.6 and 283.1 $\text{L m}^{-2} \text{h}^{-1} \text{bar}^{-1}$. These results highlight the impact of enzyme loading on catalytic performance: low enzyme concentrations limit the number of available catalytic sites, while excessively high enzyme loadings promote aggregation, which blocks mass transfer channels and reduces accessibility to active sites. This phenomenon was particularly evident in the $E_{10000}@COF-15/PAN$ membrane, which, despite its longer contact time (13.51 s), exhibited a lower conversion

rate compared to E_{5000} @COF-15/PAN. Additionally, thinner membranes, such as E_{5000} @COF-4/PAN and E_{5000} @COF-8/PAN, demonstrated significantly higher flux values of 962.5 and 619.0 L m⁻² h⁻¹ bar⁻¹, respectively. However, their conversion rates were substantially lower, at 10.2% and 27.4%, respectively. These findings suggest that catalytic activity primarily occurs within the membrane structure and emphasize the critical importance of balancing enzyme loading and membrane thickness to achieve optimal catalytic performance (Figure 3d).

To highlight the superior catalytic performance of the E_{5000} @COF-15/PAN membrane reactor, its performance was compared against both the free enzyme and the E_{5000} @COF-15 powder (derived from the membrane). Batch experiments were conducted at room temperature under stirring conditions, using reactant volumes equivalent to the permeate volume from the membrane reactor. After 30 min, the powder and the free enzyme achieved conversions of only 5.4% and 0.9%, respectively. Although longer reaction times increased the conversion rates, the rate of improvement gradually slowed. After 12 h, conversions reached 29.2% for the powder and 4.6% for the free enzyme. After 48 h, these values rose to 37.0% and 8.6%, respectively, and plateaued at 39.3% and 10.1% after 100 h. As a result, the turnover frequency (TOF) values for the free enzyme and the E_{5000} @COF-15 powder were 1018 and 254 times lower, respectively, compared to the E_{5000} @COF-15/PAN membrane bioreactor (Figure 3d,e). For a more balanced comparison, we also evaluated the TOF values of the free enzyme against E_{5000} @COF-4/PAN, which exhibited a similar conversion rate (10.1% vs. 10.2%). The TOF value of the free enzyme was 2581 times lower, further underscoring the advantages of constructing membrane bioreactors.

Kinetic studies were conducted to elucidate differences between membrane reactors and batch systems. Lineweaver–Burk plots showed excellent linearity ($R^2 > 0.99$) for both E_{5000} @COF-15/PAN and the powder, confirming adherence to Michaelis–Menten kinetics (Figures S17, S18).^[59,60] The kinetic parameters (Figure 3f) revealed that the V_{max}/K_m ratio, a measure of enzyme-substrate efficiency, was 16.8-fold higher for the membrane reactor compared to the powder. Additionally, the membrane reactor exhibited a significantly lower apparent K_m (11.9 vs. 416.7 for the powder), indicating enhanced substrate accessibility due to vacuum suction and reduced substrate retention.

To explore by-product effects, we introduced (*S*)-1-phenylethanol and acetaldehyde into the reaction mixture. In batch systems with E_{5000} @COF-15 powder, enzyme activity dropped by 25.0% in the presence of (*S*)-1-phenylethanol and 83.1% with acetaldehyde after 30 min. The efficiency gap further widened over time (Figure S19). In contrast, the membrane bioreactor exhibited minimal activity loss (4.3% and 9.7%, respectively). Subsequent washing experiments confirmed that enzyme deactivation was more pronounced in the batch system: while the membrane fully restored its activity, the powder catalyst only recovered 90% (Figure 4a). These results highlight the critical role of continuous by-product removal in maintaining enzyme performance, a key advantage of membrane-based catalysis.

Molecular dynamics (MD) simulations were conducted to examine the transport kinetics of reactants, products, and the solvent—namely 1-phenylethanol, 1-phenylethyl acetate, acetaldehyde, and hexane—through the COF-TabDma membrane (Figure S20). The results showed that hexane, serving as the solvent, exhibited the fastest transmembrane transport, followed by acetaldehyde (Figure 4b,c). The rapid diffusion of hexane increases reactant concentration within the reactor, while the efficient removal of acetaldehyde mitigates its inhibitory effects on the reaction. This differential transport behavior significantly improves the efficiency of the COF membrane reactor by maintaining elevated reactant concentrations and promoting the swift removal of reaction products. In batch systems, however, the unreacted (*S*)-1-phenylethanol and by-product acetaldehyde tend to accumulate, leading to decreased reactant availability near enzyme molecules and an increase in by-product concentration, ultimately impairing the overall reaction efficiency.

To optimize the catalytic efficiency of the E_{5000} @COF-15/PAN membrane bioreactor, we systematically examined the effects of reactant concentration and vacuum pressure. A volcano-shaped trend was observed for the TOF of 1-phenylethanol as vacuum pressure increased from 0.05 to 0.5 bar, followed by a decline when the pressure further increased to 0.9 bar (Figure 5a). This trend suggests that moderate vacuum pressure improves enzyme accessibility and maintains an optimal reactant residence time, while excessive pressure reduces residence time, thereby decreasing conversion efficiency (Figure S21). Next, we investigated the impact of varying initial 1-phenylethanol concentrations (ranging from 2.5 mM to 0.4 M) while maintaining the vinyl acetate concentration at three times that of 1-phenylethanol under the optimized vacuum pressure of 0.5 bar. The TOF increased with rising substrate concentrations but plateaued at higher concentrations due to enzyme active site saturation (Figure 5b). This behavior reflects an initial increase in enzyme-substrate collisions at lower concentrations, transitioning to a saturation phase where additional substrate no longer enhances TOF. Under these optimized conditions, the E_{5000} @COF-15/PAN membrane reactor achieved a maximum TOF of 26.8 h⁻¹ at a 1-phenylethanol concentration of 0.4 M and a vacuum pressure of 0.5 bar—setting a new benchmark for the kinetic resolution of racemic 1-phenylethanol (Figure 5c). Additionally, stability tests demonstrated that the E_{5000} @COF-15/PAN membrane retained over 95% of its initial activity after 48 h, highlighting the exceptional long-term stability of the immobilized lipase in the membrane bioreactor system (Figure S22).

To assess the versatility of the membrane bioreactor, we extended the study to the kinetic resolution of various racemic secondary alcohols using vinyl acetate as the acyl donor. Experiments were performed under optimized conditions, maintaining a vacuum pressure of 0.5 bar and a substrate concentration of 0.4 M. The E_{5000} @COF-15/PAN membrane reactor efficiently catalyzed the kinetic resolution of several racemic secondary alcohols, including 2-hexanol, 1-(4-methylphenyl)ethanol, 1-hepten-3-ol, and 1-phenyl-2-propanol, achieving TOF values between 3.1 and 26.8 h⁻¹ (Figure 5d). To further demonstrate the superior performance

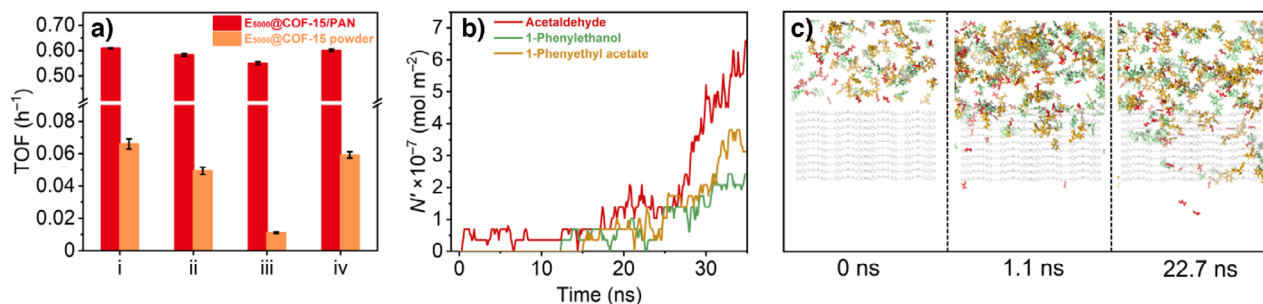


Figure 4. Demonstrating the role of mass transfer. a) Assessment of catalytic performance under various conditions: i) a mixture of 1-phenylethanol (5 mM) and vinyl acetate (15 mM) in hexane; ii) a mixture of 1-phenylethanol (5 mM), vinyl acetate (15 mM), and (*S*)-1-phenylethanol (2.5 mM) in hexane; iii) a mixture of 1-phenylethanol (5 mM), vinyl acetate (15 mM), and acetaldehyde (2.5 mM) in hexane; and iv) a hexane-washed catalytic system with 1-phenylethanol (5 mM) and vinyl acetate (15 mM) in hexane. Error bars represent the standard deviation from three independent trials for each catalytic system. b) Transmembrane molecular permeation kinetics of the reactants and products across the COF membrane, as determined by MD simulations. c) MD simulation snapshots showing the transmembrane behavior of key molecules (grey: COF-TabDma layers; green: 1-phenylethanol; red: acetaldehyde; and dark yellow: 1-phenylethyl acetate).

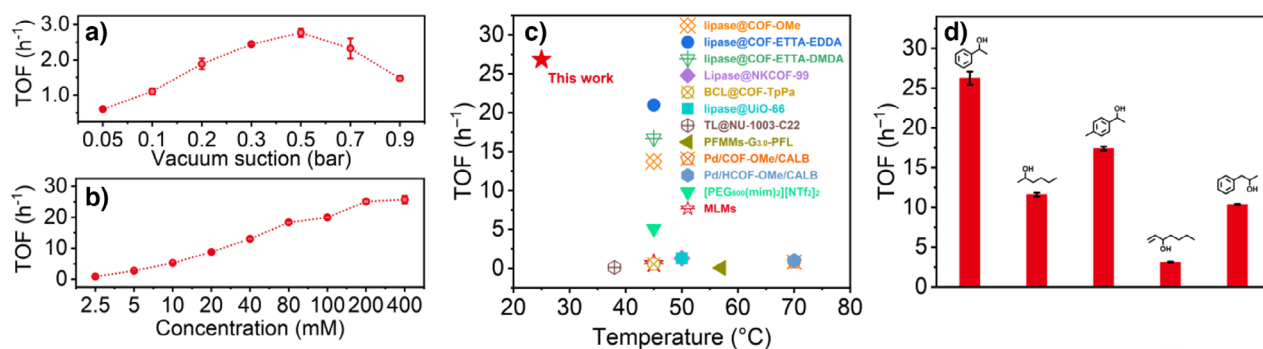


Figure 5. Comparative analysis of enzymatic performance and reaction scope. a) Investigation of the impact of vacuum suction on the TOF of E₅₀₀₀@COF-15/PAN using 1-phenylethanol (5 mM) and vinyl acetate (15 mM) in hexane. b) Analysis of the effect of varying 1-phenylethanol concentrations on the TOF of E₅₀₀₀@COF-15/PAN, maintaining vinyl acetate at three times the concentration of 1-phenylethanol under a vacuum suction of 0.5 bar. c) Comparison of the E₅₀₀₀@COF-15/PAN membrane reactor with other catalytic systems documented in Table S1. d) Evaluation of the catalytic performance of the E₅₀₀₀@COF-15/PAN membrane in the kinetic resolution of various racemic secondary alcohols. Error bars represent the standard deviation from three independent trials for each catalytic system.

of the membrane bioreactor, we applied it to the alcoholysis of aspirin methyl ester to produce methyl salicylate, a key intermediate in the chemical industry.^[61] The E₅₀₀₀@COF-15/PAN membrane reactor achieved an impressive TOF of 17.3 h⁻¹ when using a 1 M aspirin methyl ester ethanol solution as the reactant, operating under a vacuum pressure of 0.3 bar. In contrast, the corresponding powder biocomposite resulted in a conversion of 12.1% after 3 h, while free lipase achieved a conversion of only 8.8% after 100 h. Accordingly, the TOF values were calculated as 17.3 h⁻¹ for E₅₀₀₀@COF-15/PAN, 2.87 h⁻¹ for E₅₀₀₀@COF-15 powder, and 0.06 h⁻¹ for free lipase (Figures 6a and S23–S25).

Conclusion

In summary, this study underscores the exceptional potential of COF nanosheets as substrates for enzyme immobilization, paving the way for the development of highly efficient membrane bioreactors. The innovative layer-by-layer assembly technique presented here successfully addresses persistent challenges, including: aligning pore channel dimensions with

enzyme molecule sizes and avoiding unfavorable chemical conditions during chemical modification or de novo assembly. Furthermore, the intrinsic porosity and interlayer spacing of COF nanosheets significantly enhance reactant accessibility, while the continuous membrane catalysis system mitigates enzyme exposure to harmful chemicals. This design not only improves catalytic efficiency and minimizes by-product inhibition but also ensures long-term operational stability—a key advantage over conventional batch systems.

The adaptability of this approach is further demonstrated by its successful application to various enzymes. For example, lysozyme, a widely used enzyme, was effectively incorporated into membrane reactors (Lysozyme@COF/PAN) using the same strategy, showing superior enzymatic efficiency compared to both the corresponding powder form (Lysozyme@COF) and the free enzyme (Figures 6b, and S26–S30). Specifically, Lysozyme@COF/PAN, Lysozyme@COF, and free lysozyme achieved conversion rates of 85.2%, 49.0%, and 27.4%, respectively, in the hydrolysis of chitobiose. Moreover, the flexibility of this method, combined with the broad range of molecular building blocks available for COF synthesis, enables the

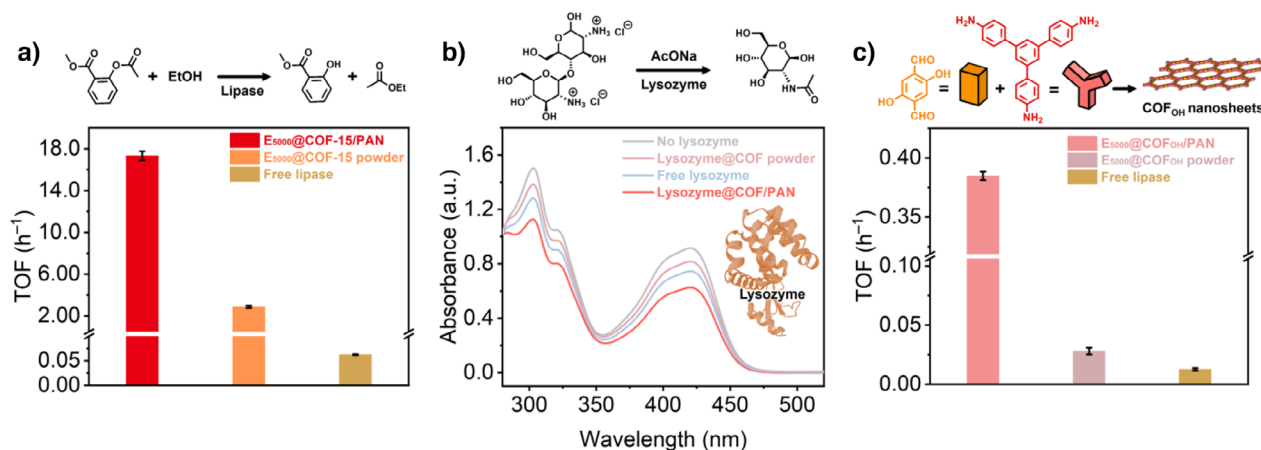


Figure 6. Superior catalytic performance of the membrane bioreactor and the versatility of the layer-by-layer assembly strategy for different enzymes and COF nanosheets. a) Reaction scheme for the hydrolysis of methyl aspirin, along with a comparison of catalytic efficiencies across different systems. b) Reaction scheme for the hydrolysis of chitobiose, along with UV-vis spectra of various catalysts in the hydrolysis of chitobiose in 0.1 M acetate buffer. A decrease in absorbance at 420 nm correlates with an increase in enzymatic activity. c) Synthetic pathway for COF_{OH} nanosheets and a comparison of catalytic efficiency between the corresponding membrane bioreactor, powder biocomposite, and free lipase. Error bars represent the standard deviation from three independent trials for each catalytic system.

tailored design of microenvironments optimized for specific enzymatic reactions. For example, lipase was immobilized using COF_{OH} nanosheets synthesized from Tab and 2,5-dihydroxyterephthalaldehyde. While this system showed slightly lower catalytic efficiency compared to the COF-TabDma-based membrane bioreactor—specifically in the kinetic resolution of racemic secondary alcohols and the alcoholysis of aspirin methyl ester—this behavior is consistent with previous findings that lipase activity is enhanced in hydrophobic environments (Figure 6c, and S31–S36). Nevertheless, the resulting membrane bioreactor significantly outperformed both the powder counterpart and the free enzyme under batch conditions (Figures S37). Moreover, the COF membrane bioreactor maintained its stability during catalysis, as shown by the intact morphology (Figure S38). Overall, this work establishes a solid foundation for the precise engineering of advanced membrane bioreactors, addressing key challenges in biocatalyst immobilization. By enabling scalable, efficient, and sustainable biocatalytic processes, this approach opens new avenues for diverse applications in industrial biotechnology and beyond.

Supporting Information

The authors have cited additional references within the Supporting Information.

Acknowledgements

This work was supported by the National Key Research and Development Program of China (2022YFA1503004), the National Science Foundation of China (22072132 and 22472152), and the National Science Foundation of Zhejiang province (LR23B060001). The authors appreciate the assistance of Fang Chen from Analytical Testing Center of the

Department of Chemistry, Zhejiang University, in conducting SEM measurements.

Conflict of Interests

The authors declare no conflict of interest.

Data Availability Statement

The data that support the findings of this study are available in the Supporting Information of this article.

Keywords: Biocatalysis • Covalent • Enzyme immobilizing • Layer-by-layer assembly • Membrane bioreactors • Organic framework membrane

- [1] M. A. Huffman, A. Fryszkowska, O. Alvizo, M. Borra-Garske, K. R. Campos, K. A. Canada, P. N. Devine, D. Duan, J. H. Forstater, S. T. Grosser, H. M. Halsey, G. J. Hughes, J. Jo, L. A. Joyce, J. N. Kolev, J. Liang, K. M. Maloney, B. F. Mann, N. M. Marshall, M. McLaughlin, J. C. Moore, G. S. Murphy, C. C. Nawrat, J. Nator, S. Novick, N. R. Patel, A. Rodriguez-Granillo, S. A. Robaire, E. C. Sherer, M. D. Truppo, et al., *Science* **2019**, *366*, 1255–1259.
- [2] M. T. Reetz, G. Qu, Z. Sun, *Nat. Synth.* **2024**, *3*, 19–32.
- [3] S. L. Lovelock, R. Crawshaw, S. Basler, C. Levy, D. Baker, D. Hilvert, A. P. Green, *Nature* **2022**, *606*, 49–58.
- [4] R. Buller, S. Lutz, R. J. Kazlauskas, R. Snajdrova, J. C. Moore, U. T. Bornscheuer, *Science* **2023**, *382*, eadh8615.
- [5] Y. Zhang, Z. Xiong, Y. Li, M. Wilson, K. E. Christensen, E. Jaques, P. Hernández-Lladó, J. Robertson, L. L. Wong, *Nat. Synth.* **2022**, *1*, 936–945.
- [6] G. Chen, S. Huang, X. Ma, R. He, G. Ouyang, *Nat. Protoc.* **2023**, *18*, 2032–2050.

- [7] C. Hu, Y. Bai, M. Hou, Y. Wang, L. Wang, X. Cao, C.-W. Chan, H. Sun, W. Li, J. Ge, K. Ren, *Sci. Adv.* **2020**, *6*, eaax5785.
- [8] H. Lu, J. Ouyang, W.-Q. Liu, C. Wu, J. Li, *Angew. Chem., Int. Ed.* **2023**, *62*, e202312906.
- [9] J. Ouyang, Z. Zhang, J. Li, C. Wu, *Angew. Chem., Int. Ed.* **2024**, *63*, e202400105.
- [10] H. Ma, X. Liu, A. H. Nobbs, A. Mishra, A. J. Patil, S. Mann, *Adv. Mater.* **2024**, *36*, 2404607.
- [11] L. Guo, R. He, G. Chen, H. Yang, X. Kou, W. Huang, R. Gao, S. Huang, S. Huang, F. Zhu, G. Ouyang, *J. Am. Chem. Soc.* **2024**, *146*, 17189–17200.
- [12] M. Li, S. Qiao, Y. Zheng, Y. H. Andaloussi, X. Li, Z. Zhang, A. Li, P. Cheng, S. Ma, Y. Chen, *J. Am. Chem. Soc.* **2020**, *142*, 6675–6681.
- [13] M. Liu, L. Chen, Z. Zhao, M. Liu, T. Zhao, Y. Ma, Q. Zhou, Y. S. Ibrahim, A. A. Elzatahry, X. Li, D. Zhao, *J. Am. Chem. Soc.* **2022**, *144*, 3892–3901.
- [14] Y. Zhang, C. Xing, Z. Mu, Z. Niu, X. Feng, Y. Zhang, B. Wang, *J. Am. Chem. Soc.* **2023**, *145*, 13469–13475.
- [15] S. Dutta, N. Kumari, S. Dubbu, S. W. Jang, A. Kumar, H. Ohtsu, J. Kim, S. H. Cho, M. Kawano, I. S. Lee, *Angew. Chem., Int. Ed.* **2020**, *59*, 3416–3422.
- [16] P. Li, J. A. Modica, A. J. Howarth, E. Vargas, L. Peyman, Z. Moghadam, R. Q. Snurr, M. Mrksich, J. T. Hupp, O. K. Farha, *Chem* **2016**, *1*, 154–169.
- [17] R. Gao, X. Kou, L. Tong, Z.-W. Li, Y. Shen, R. He, L. Guo, H. Wang, X. Ma, S. Huang, G. Chen, G. Ouyang, *Angew. Chem., Int. Ed.* **2024**, *63*, e202319876.
- [18] J. Liang, J. Ruan, B. Njelic, A. Rawal, J. Scott, J. Xu, C. Boyer, K. Liang, *Angew. Chem., Int. Ed.* **2023**, *62*, e202303001.
- [19] T. Man, C. Xu, X.-Y. Liu, D. Li, C.-K. Tsung, H. Pei, Y. Wan, L. Li, *Nat. Commun.* **2022**, *13*, 305.
- [20] M. Feng, Z. Niu, C. Xing, Y. Jin, X. Feng, Y. Zhang, B. Wang, *Angew. Chem., Int. Ed.* **2023**, *62*, e202306621.
- [21] D. Zheng, Y. Zheng, J. Tan, Z. Zhang, H. Huang, Y. Chen, *Nat. Commun.* **2024**, *15*, 5510.
- [22] J.-S. Bae, E. Jeon, S.-Y. Moon, W. Oh, S.-Y. Han, J. H. Lee, S. Y. Yang, D.-M. Kim, J.-W. Park, *Angew. Chem., Int. Ed.* **2016**, *55*, 11495–11498.
- [23] N. Moridi, P. F.-X. Corvini, P. Shahgaldian, *Angew. Chem., Int. Ed.* **2015**, *54*, 14800–14804.
- [24] V. R. R. Marthala, M. Friedrich, Z. Zhou, M. Distaso, S. Reuss, S. A. Al-Thabaiti, W. Peukert, W. Schwieger, M. Hartmann, *Adv. Funct. Mater.* **2015**, *25*, 1832–1836.
- [25] Y. Wang, H. Zhang, R. Fan, Y. Wan, M. Huang, S. Huang, L. Pan, J. Luo, *Chem. Eng. Sci.* **2024**, *293*, 120077.
- [26] P. Jochems, Y. Satyawali, L. Diels, W. Dejonghe, *Green Chem.* **2011**, *13*, 1609.
- [27] R. Mazzei, A. Yidego Gebreyohannes, T. Poerio, V. Sansone, V. Musteata, L. Upadhyaya, L. Bruno, R. Gorecki, S. P. Nunes, L. Giorno, *J. Membr. Sci.* **2024**, *700*, 122708.
- [28] H. Zhang, J. Luo, J. M. Woodley, Y. Wan, *Chem. Eng. J.* **2021**, *421*, 127870.
- [29] D. J. Bell, M. Wiese, A. A. Schönberger, M. Wessling, *Angew. Chem., Int. Ed.* **2020**, *59*, 16047–16053.
- [30] Z. Guo, H. Jiang, H. Wu, L. Zhang, S. Song, Y. Chen, C. Zheng, Y. Ren, R. Zhao, Y. Li, Y. Yin, M. D. Guiver, Z. Jiang, *Angew. Chem., Int. Ed.* **2021**, *60*, 27078–27085.
- [31] D. Rodríguez-San-Miguel, C. Montoro, F. Zamora, *Chem. Soc. Rev.* **2020**, *49*, 2291–2302.
- [32] E. Vargo, L. Ma, H. Li, Q. Zhang, J. Kwon, K. M. Evans, X. Tang, V. L. Tovmasyan, J. Jan, A. C. Arias, H. Destailats, I. Kuzmenko, J. Ilavsky, W.-R. Chen, W. Heller, R. O. Ritchie, Y. Liu, T. Xu, *Nature* **2023**, *623*, 724–731.
- [33] L. Huang, W. Li, F. Wei, S. Ke, H. Chen, C. Jing, J. Cheng, S. Liu, *Chem* **2024**, *10*, 3100–3113.
- [34] K. Koner, H. S. Sasmal, D. Shetty, R. Banerjee, *Angew. Chem., Int. Ed.* **2024**, *63*, e202406418.
- [35] W. Liu, X. Li, C. Wang, H. Pan, W. Liu, K. Wang, Q. Zeng, R. Wang, J. Jiang, *J. Am. Chem. Soc.* **2019**, *141*, 17431–17440.
- [36] T. Huang, H. Jiang, J. C. Douglin, Y. Chen, S. Yin, J. Zhang, X. Deng, H. Wu, Y. Yin, D. R. Dekel, M. D. Guiver, Z. Jiang, *Angew. Chem., Int. Ed.* **2023**, *62*, e202209306.
- [37] X. Wu, X. Han, Q. Xu, Y. Liu, C. Yuan, S. Yang, Y. Liu, J. Jiang, Y. Cui, *J. Am. Chem. Soc.* **2019**, *141*, 7081–7089.
- [38] Y. Liu, J. Ren, Y. Wang, X. Zhu, X. Guan, Z. Wang, Y. Zhou, L. Zhu, S. Qiu, S. Xiao, Q. Fang, *CCS Chem* **2023**, *5*, 2033–2045.
- [39] Y.-J. Chen, M. Liu, J. Chen, X. Huang, Q.-H. Li, X.-L. Ye, G.-E. Wang, G. Xu, *Chem. Sci.* **2023**, *14*, 4824–4831.
- [40] J.-H. Lee, H. Lee, J. Lee, T. W. Kang, J. H. Park, J.-H. Shin, H. Lee, D. Majhi, S. U. Lee, J.-H. Kim, *ACS Nano* **2023**, *17*, 17372–17382.
- [41] E. Zhou, X. Zhang, L. Zhu, E. Chai, J. Chen, J. Li, D. Yuan, L. Kang, Q. Sun, Y. Wang, *Sci. Adv.* **2024**, *10*, eadk8564.
- [42] W. Wei, S. Zhou, D.-D. Ma, Q. Li, M. Ran, X. Li, X.-T. Wu, Q.-L. Zhu, *Adv. Funct. Mater.* **2023**, *33*, 2302917.
- [43] G. Yu, Y. Cui, S. Lin, R. Liu, S. Liu, Y. Zhu, D. Wu, *Adv. Funct. Mater.* **2024**, *34*, 2314935.
- [44] Z. Guo, H. Wu, Y. Chen, S. Zhu, H. Jiang, S. Song, Y. Ren, Y. Wang, X. Liang, G. He, Y. Li, Z. Jiang, *Angew. Chem., Int. Ed.* **2022**, *61*, e202210466.
- [45] H. Kim, Y. K. Choi, J. Lee, E. Lee, J. Park, M.-J. Kim, *Angew. Chem., Int. Ed.* **2011**, *50*, 10944–10948.
- [46] L. Wang, A. C. Hortelão, X. Huang, S. Sánchez, *Angew. Chem., Int. Ed.* **2019**, *58*, 7992–7996.
- [47] K. Li, J. Wang, Y. He, G. Cui, M. A. Abdulrazaq, Y. Yan, *Chem. Eng. J.* **2018**, *351*, 258–268.
- [48] H. Xu, J. Gao, D. Jiang, *Nat. Chem.* **2015**, *7*, 905–912.
- [49] Q. Sun, Y. Tang, B. Aguila, S. Wang, F.-S. Xiao, P. K. Thallapally, A. M. Al-Enizi, A. Nafady, S. Ma, *Angew. Chem., Int. Ed.* **2019**, *58*, 8670–8675.
- [50] Q. Sun, C.-W. Fu, B. Aguila, J. Perman, S. Wang, H.-Y. Huang, F.-S. Xiao, S. Ma, *J. Am. Chem. Soc.* **2018**, *140*, 984–992.
- [51] Q. Sun, B. Aguila, P. C. Lan, S. Ma, *Adv. Mater.* **2019**, *31*, 1900008.
- [52] H. Liu, Y. Zhou, J. Guo, R. Feng, G. Hu, J. Pang, Y. Chen, O. Terasaki, X.-H. Bu, *J. Am. Chem. Soc.* **2023**, *145*, 23227–23237.
- [53] Y. Zheng, S. Zhang, J. Guo, R. Shi, J. Yu, K. Li, N. Li, Z. Zhang, Y. Chen, *Angew. Chem., Int. Ed.* **2022**, *61*, e202208744.
- [54] A. Park, S. Park, *ACS Catal.* **2022**, *12*, 2397–2402.
- [55] J. Wang, K. Li, Y. He, Y. Wang, J. Yan, L. Xu, X. Han, Y. Yan, *ACS Appl. Mater. Interfaces* **2020**, *12*, 4906–4916.
- [56] Y. Feng, R. Shi, M. Yang, Y. Zheng, Z. Zhang, Y. Chen, *Angew. Chem., Int. Ed.* **2023**, *62*, e202302436.
- [57] L. Zheng, Z. Zhang, Z. Lai, S. Yin, W. Xian, Q.-W. Meng, Z. Dai, Y. Xiong, X. Meng, S. Ma, F.-S. Xiao, Q. Sun, *Nat. Commun.* **2024**, *15*, 6837.
- [58] X. Li, S. Pang, Y. Zhang, J. Fu, G. He, B. Song, D. Peng, X. Zhang, L. Jiang, *Adv. Mater.* **2024**, *36*, 2310954.
- [59] C. Xing, P. Mei, Z. Mu, B. Li, X. Feng, Y. Zhang, B. Wang, *Angew. Chem., Int. Ed.* **2022**, *61*, e202201378.
- [60] L. Hao, Q. Zhu, X. Qiao, Q. Shi, Y. Liu, T. Wang, E. Lin, C. Peng, Z. Zhang, Y. Chen, *Angew. Chem., Int. Ed.* **2024**, *63*, e202416550.
- [61] P. P. Chiplunkar, X. Zhao, P. D. Tomke, J. Noro, B. Xu, Q. Wang, C. Silva, A. P. Pratap, A. Cavaco-Paulo, *Ultrason. Sonochem.* **2018**, *40*, 587–593.

Manuscript received: March 12, 2025
Revised manuscript received: April 10, 2025
Accepted manuscript online: April 30, 2025
Version of record online: May 06, 2025